Surface-Enhanced Resonance Raman Scattering (SERRS) Using Au Nanohole Arrays on Optical Fiber Tips

**Gustavo F. S. Andrade · Juliano G. Hayashi ·
Mohammad M. Rahman · Walter J. Salcedo ·
Cristiano M. B. Cordeiro · Alexandre G. Brolo**

Abstract Circular and bow tie-shaped Au nanoholes arrays were fabricated on gold films deposited on the tips of single-mode optical fibers. The nanostructures were milled using focused ion beam with a high quality control of their shapes and sizes. The optical fiber devices were used for surface-enhanced resonance Raman scattering (SERRS) measurements in both back- and forward-scattering geometries, yielding promising performance in both detection arrangements. The effect of the hole shape on the SERRS performance was explored with the bow tie nanostructures presenting a better SERRS performance than the circular holes arrays. The results present here are another step towards the development of optical fiber tips modified with plasmonic nanostructures for SERRS applications.

Keywords Nanoplasmonic structures · Surface-enhanced Raman scattering · SERRS sensing · Single-mode optical fibers

G. F. S. Andrade · M. M. Rahman · A. G. Brolo (✉)
Department of Chemistry, University of Victoria, PO Box 3055,
Victoria, BC, Canada V8W 3P6
e-mail: agbrolo@uvic.ca

J. G. Hayashi · C. M. B. Cordeiro (✉)
Instituto de Física "Gleb Wataghin", Universidade Estadual
de Campinas—UNICAMP, Campinas, SP, Brazil
e-mail: cmbc@ifi.unicamp.br

G. F. S. Andrade (✉)
Instituto de Ciências Exatas, Departamento de Química,
Universidade Federal de Juiz de Fora, Campus Universitário s/n,
CEP 36036-900, Juiz de Fora, Brazil
e-mail: gustavo.andrade@ufjf.edu.br

W. J. Salcedo
Departamento de Sistemas Eletrônicos da Escola politécnica,
Universidade de São Paulo, São Paulo, Brazil

Introduction

Optical fibers are one of the greatest technological breakthroughs of the last 50 years. They are widely used in the transport of light for many applications that directly impact our everyday life, such as in telecommunications. The use of optical fibers in analytical chemistry has also grown strongly in the last few years due to their great flexibility as either light carriers or analytical platforms [1]. The use of optical fibers for remote sensing has been explored, which allows for a much more flexible sensor when compared to planar optical platforms.

Applications of optical fibers coupled to surface plasmon and Raman-based techniques have also been reported [2, 3]. Surface plasmon is the collective movement of electrons in a metal surface that can be excited by light and result in an enhancement of the local electromagnetic field at the metal–dielectric interface. Enhanced optical spectroscopic methods, such as surface-enhanced Raman scattering (SERS), are among the important consequences of the enormous field enhancement observed at metallic nanostructured surfaces. The SERS effect was discovered almost 40 years ago [4–6], and it consists of a large increase in the Raman cross section for molecules in contact to those nanostructures that support surface plasmon resonance (SPR). Chemical applications of SERS range from spectroelectrochemistry [7, 8] to biosensing [9–12]. The SERS technique is actually one of the few optical spectroscopic methods able to detect single molecules [13, 14]. Such great flexibility and sensitivity make SERS a very interesting tool for both qualitative [15] and quantitative analysis [16, 17]. As mentioned above, the most significant contribution to the enhancement of the Raman cross section in the SERS effect is the excitation of surface plasmons [18, 19], which causes great localization of the electric field in very small regions [20]. However, when the laser line (used as

excitation source in Raman measurements) matches an internal electronic transition of the adsorbed molecule, there is an additional enhancement of the Raman signal due to the resonance Raman phenomenon; the resulting effect combines both SERS and resonance Raman and it is named surface-enhanced resonance Raman scattering (SERRS) [21, 22].

The integration of SERS with optical fibers has been receiving an important amount of attention in the last few years [23–28]. There is a wide variety of reports on approaches to use optical fibers in SERS. These include the use of optical fibers simply as light carriers for SERS measurements from nanoparticle suspension, the etching of the cladding of optical fibers and modification with metallic films in order to take advantage of the evanescent field that is produced during light propagation, and the use of optical fiber tips modified with sensing layers [23–28]. The modification of the tip of optical fibers with metallic nanostructures for SERS have been achieved by several methods, including the immobilization of alumina particles covered with Ag layers [29], sol–gel deposition of Ag-NPs [30], photochemical reduction of Ag on the optical fiber tip [31], nanoimprinting using cicada wings as templates [32], and nanolithographic fabrication of Au nanostructures [33]. The common objective of the preceding works was to build a very flexible platform for remote sensing, with a smaller sensing area and optimized performance relative to the typical planar substrates.

Our group has previously reported on the use of arrays of nanoholes on Au (AuNHA) films as SPR and SERS substrates [34, 35]. The AuNHA proved to be very useful for the detection of biologically significant species by SPR [36], and it was also possible to show that the SERS performance can be enhanced by changing the geometric parameters of the nanostructures, including the shape of the nanoholes [37, 38]. Recently, Au nanoislands were milled on gold films deposited on cleaved optical fiber tips and the use of that device as SPR sensors for bulk refractive index of solvents was reported [39]. The integration of AuNHA with optical fiber detection is an important step forward in SERS research because this procedure may allow a higher degree of reproducibility than any previously reported device. In addition, AuNHA may result in new levels of stability of the SERS substrate, allowing for applications in harsh environments.

In the present work, AuNHA were milled on the tips of single-mode (in the visible range) optical fibers (AuNHA-OFT). Arrays with holes with two different shapes, circular and bow tie-shaped, were milled. The performances of the resulting devices as SERRS substrates were evaluated.

Experimental Section

Chemicals

Ultrapure water with a resistivity of 18.2 MΩcm (Barnstead NANOpure Diamond water purification system) was used throughout the experiments. Methanol and ethanol were obtained from Calderon and they were used without further purification. Oxazine 720 (Oxa) was obtained from Lambdachrome.

AuNHA-OFT Fabrication

The fabrication of the AuNHA was described in details elsewhere [34]. Briefly, samples of arrays of nanoholes were fabricated on the tips of optical fibers by focused ion beam (FIB) using two equipment: a FEI 235 dual beam focused ion beam and field emission scanning electron microscope and a FEI Nova 200 Nanolab Dual Beam focused ion beam and scanning electron microscope. The gallium ion beam was set to a typical applied voltage of 30 keV and 100 pA of beam current for milling. The nanoholes were milled on a 100-nm gold film deposited on a 3-nm Cr adhesion layer. Both Cr and Au were deposited by thermal evaporation on the tip of a single-mode optical fiber (Newport, F-SA, core diameter 3.4 μm). The circular nanoholes were 200 nm in diameter, and the array periodicity was 480 nm. The bow tie nanoholes were 200 nm in height, 420 nm in the bottom side, and the separation between the triangles was 95 nm. Each circular nanohole array contained 30×30 nanoholes and occupied an area of ca. 16×16 μm^2 with a fill factor of 13 %. Each bow tie nanoholes array contained 40×40 bow tie nanostructures in an area of ca. 20×20 μm^2 and a fill factor of 23 %. The spot of the laser used in the SERS experiments had a diameter of 2 μm, and the Raman mapping technique was used to obtain the spatial distribution of SERS intensities from the whole arrays, as it has been done in previous works [30]. It is worth noticing that the area of the fiber core was around 9.1 μm^2, considerably smaller than the area occupied by the array of nanoholes. Hence, with the correct positioning, the arrays of nanoholes completely covered the core area, which means that the light transmitted by the fiber had to go through the arrays. The nanohole arrays were characterized by white light transmission. The transmission spectra of the fibers with a circular hole array presented a maximum at 638 nm, which is in agreement to previous reports from our group. Figure 1 presents the SEM images of the circular and bow tie nanoholes arrays milled on the optical fiber tips.

SERS Experiments

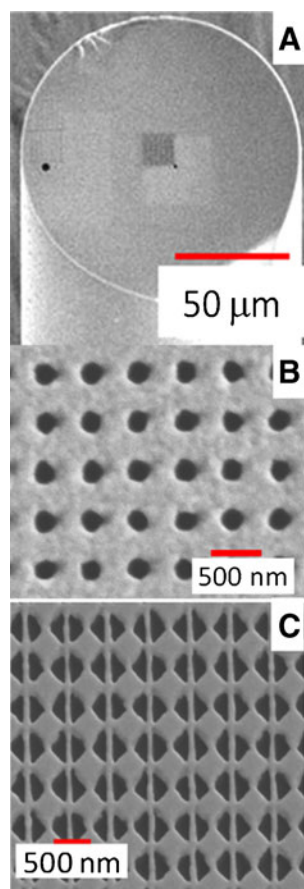The SERS measurements were performed in a Renishaw inVia Raman microscope system equipped with a He-Ne

Fig. 1 Scanning electron micrographs (SEM) of optical fiber tips modified with arrays of nanoholes on Au films. **a** Low magnification SEM of an optical fiber tip containing an array of circular nanoholes at the tip center; **b** high-magnification SEM of an array of circular holes on an optical fiber tip; **c** high-magnification SEM of an array of bow tie nanoholes on an optical fiber tip

laser source with excitation at 632.8 nm. The laser power on the sample was 0.4 mW, and the laser spot area was ~3 μm^2. The SERS probe used was Oxa, a laser dye resonant with the He-Ne laser line at 633 nm. Therefore, all the spectra had an additional contribution from the resonance Raman effect and the acronyms SERRS will then be used throughout the text. It should also be noticed that the 633 nm laser line is also in resonance with the LSPR resonance of the AuNHA. An ethanolic solution of 10 μM Oxa was drop cast on the AuNHA-OFT and allowed to dry, and then the devices were thoroughly washed with deionized water. The SERRS measurements were then made in two different acquisition geometries, forward-scattering and back-scattering. Figure 2 presents a scheme for the experimental setups. In the forward-scattering measurement (left hand side in Fig. 2), the laser light was coupled to the unmodified distal tip of the fiber, and the scattered light was collected with the Renishaw microscope at the AuNHA-modified tip. In this arrangement, the excitation light must be transmitted through the nanoholes to excite the adsorbed molecules. In

the back-scattering experiment, the AuNHA-OFT was mounted in the microscope stage of the spectrometer, and the exciting light hit the arrays of nanoholes directly. The scattered light was collected back into the spectrometer with the same objective used for excitation. The back-scattering data (right hand side in Fig. 2) were acquired by SERRS mapping to compare the enhancement of the Raman intensity in and out the area containing the AuNHA. In mapping experiments, the computer-controlled stage was scanned in 1 μm steps (in both horizontal and vertical directions), so the excitation laser can probe a predefined area of the optical fiber tip. SERRS spectra were taken from each point in the predetermined area spatially defined by the size of the laser beam. After these spectra were obtained, the SERRS intensity of the band at 594 cm^{-1} of the Oxa dye was arranged in a 2-D plot correlating with the position from where each spectrum was obtained. A third experimental arrangement, called optrode mode, was also attempted. This configuration consists of excitation similar to the forward-scattering geometry but with the scattered light measured at the same (unmodified) tip. However, the signal obtained using the optrode geometry was heavily contaminated with Raman scattering contributions from the glass matrix of the fiber and the results obtained using that geometry are not presented in this work.

Finite-Difference Time-Domain Calculations

The theoretical electric near-field spectra of the nanohole arrays were calculated using the 3D FDTD method. The calculations were performed using the commercially available Lumerical® software. The nanostructures were placed on a glass substrate with the same refractive index of the fiber optics core (n=1.53). The refractive index of gold and Cr were from the sources indicated in the Lumerical software.

Results and Discussion

AuNHA-OFT Characterization

The fabrication of the Au nanoholes array on the optical fiber tip (AuNHA-OFT) was performed by FIB milling of an Au layers thermally deposited on freshly cleaved fiber tips. The arrays of nanoholes were milled on the geometrical center of the fiber cross section, where the fiber core is found. Figure 1a presents the SEM image at low magnification of an AuNHA-OFT device; in the figure, one can notice the dark spot on the middle of the optical fiber tip, on top of the fiber core that corresponds to the AuNHA. Figure 1b, c shows the typical SEM images of circular and bow tie arrays of nanoholes with a higher magnification.
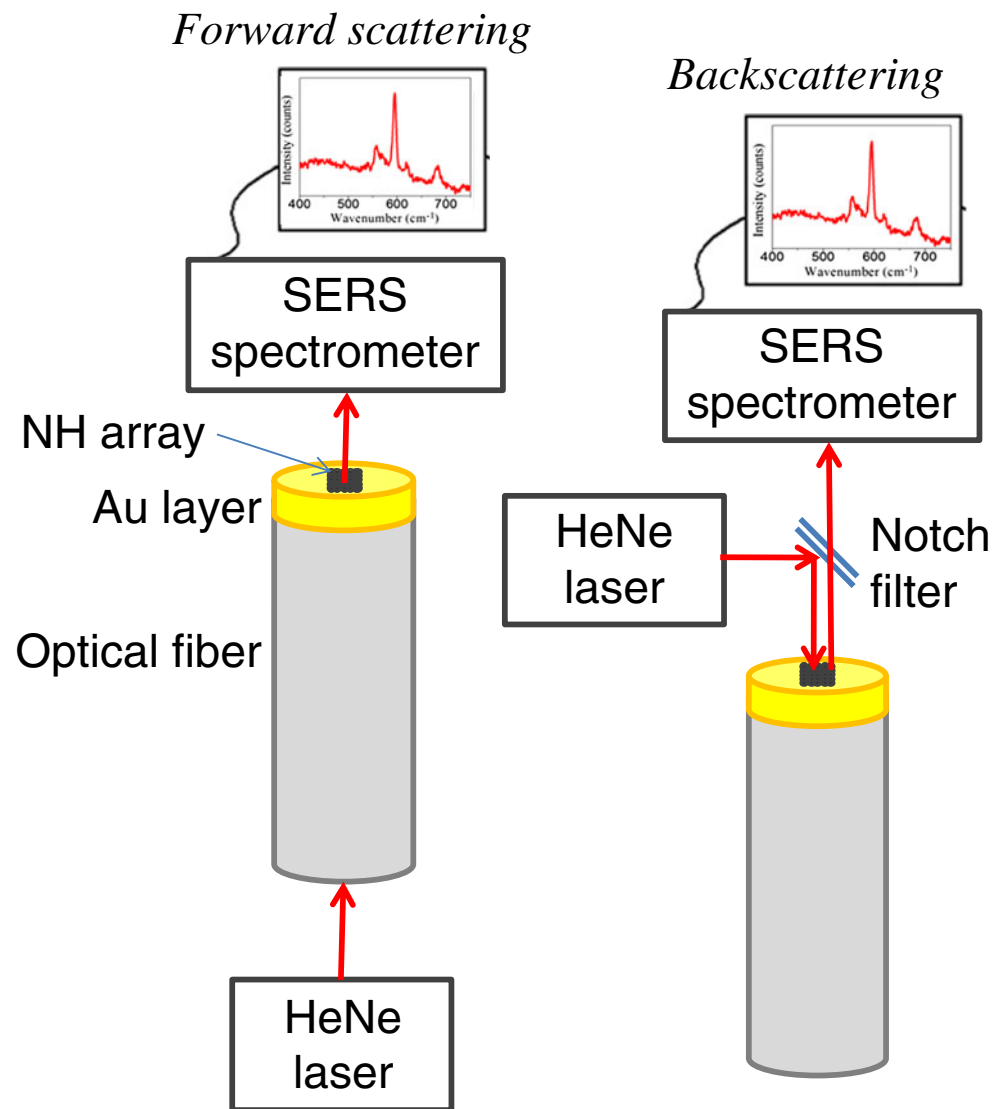
It is important to clarify that the SEM images reported in Fig. 1 are from a subset that are representative of several other fabricated samples (more than 10 samples for either circular and bow tie-shaped holes). The SERRS mappings and spectra reported in the following sections are also taken to be representative of several samples, in order to assure that the well-known reproducibility of AuNHA-based surfaces [36–38] (around 10 % sample to sample variation) are adequately met.

SERRS from AuNHA-OFT

The plasmonic properties of the arrays of nanoholes on gold enable enhanced spectroscopy, including the SERRS effect [35]. The SERRS intensity is dependent on the size and shape of the nanoholes, on the period-icity of the arrays and on the thickness of the Au film [35, 37, 38].

Figure 3a presents a SERRS mapping of Oxa on the circular AuNHA-OFT, obtained using the back-scattering geometry, superimposed to the optical microscopy image of the sample. Figure 3b presents two spectra from different points in the mapping shown in Fig. 3a. The brighter colors in the SERRS mapping in Fig. 3a indicate higher Raman intensities. The mapping was set to partially cover the AuNHA and to also probe the surrounding Au film. Figure 3c provides then a comparison between the spatially averaged SERRS intensities obtained for surrounding Au film. The averages and the standard deviations of the spatial distribution of SERRS intensities associated with the two sets of data are also presented in Fig. 3c. It is noticeable that SERRS intensity is consistently more intense on the nanoholes array than for the Au film surrounding the array. The average SERRS intensity measured in the circular AuNHA in Fig. 3c is 2.7 times larger than the average in the Au film. The spatial variation of the intensities was
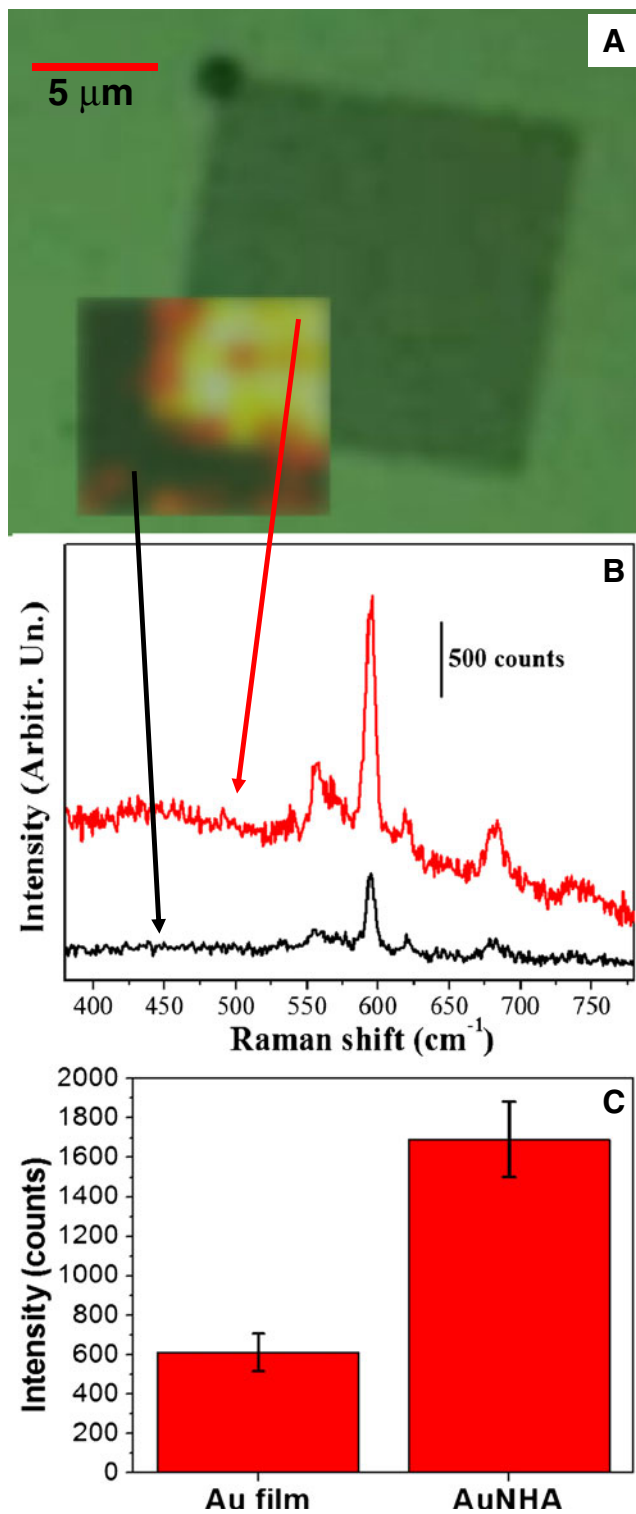
Fig. 3 **a** SERRS mapping of the Oxa 594 cm^{-1} band superimposed to the optical image of an AuNHA-OFT; **b** SERRS spectra corresponding to two points in the SERRS mapping indicated by the *arrows*. **c** The average SERRS intensity on the circular AuNHA and on the surrounding Au film. The averaging was over 228 samples for the AuNHA and 134 samples for the Au film. The *error bars* in the figures corresponds to twice the standard deviation of the measurements

around 15 % for both the patterned and unpatterned regions. The fact that significant SERRS intensities were observed from the unpatterned Au film is attributed to the roughness of the thermally evaporated Au combined to the intrinsic resonance Raman effect of Oxa [40]. The patterned region of the arrays should allow a controllable enhancement of the SERRS performance. Although the increase for circular hole arrays seems modest, it is important to point out that the enhancement is relative to a rough Au surface, which is known to provide an increase in Raman efficiency of about 10^6. On the other hand, the ca. 3× increase could be attributed just to an increase in roughness introduced during the preparation of the circular nanohole patterning. It should be pointed out that a previous work indicated that the actual enhancement that arises solely from the AuNHA is in the order of 10 [2, 3, 41].

In order to try to improve the SERRS efficiency and confirm that the relative enhancement was indeed the effect of the nanostructure, the SERRS measurements were also performed on a designed bow tie AuNHA-OFT device. It can be noticed that the bow tie AuNHA-OFT is an anisotropic structure, so the polarization of the excitation laser relative to the orientation of the nanostructure is expected to result in different SERRS performance [37]. This polarization effect should be absent if the relative enhancement on the nanostructured area originates only from an increase in regular roughness of the film. Therefore, polarization measurements allow the quantification of the effect due solely to the nanostructure on the SERRS performance.

Figure 4a, b presents the mapping of a bow tie AuNHA-OFT device for two perpendicular laser polarizations, and Fig. 4c presents the spatially averaged SERRS intensity on the bow tie AuNHA-OFT and on the Au thin film for both polarizations. The insert in Fig. 4c presents the orientation of the bow tie structures for these measurements, and one can notice that the laser polarization is parallel to the triangle basis in Fig. 4a and perpendicular to the basis in Fig. 4b. The SERRS intensity map in Fig. 4a (laser polarization parallel to the triangular basis of the bow tie structures) presents a small difference in intensities moving from the bow tie AuNHA-OFT to the Au thin film, as can be clearly seen in Fig. 4c, which shows that, for this polarization, the region on the bow tie AuNHA-OFT is 1.8 times higher than for the Au thin film, but both values present high standard deviation. On the other hand, Fig. 4b presents the SERRS intensity map for the bow tie AuNHA-OFT obtained using the laser polarization perpendicular to the basis of the bow tie structures. The mapping in Fig. 4b shows that the SERRS intensity from the bow tie AuNHA is considerably stronger than on the Au film. Figure 4c shows that the spatially averaged intensity on the bow tie AuNHA region for perpendicular polarization is 3.6 times larger than on the Au film, a 40 % improvement compared to the circular AuNHA.
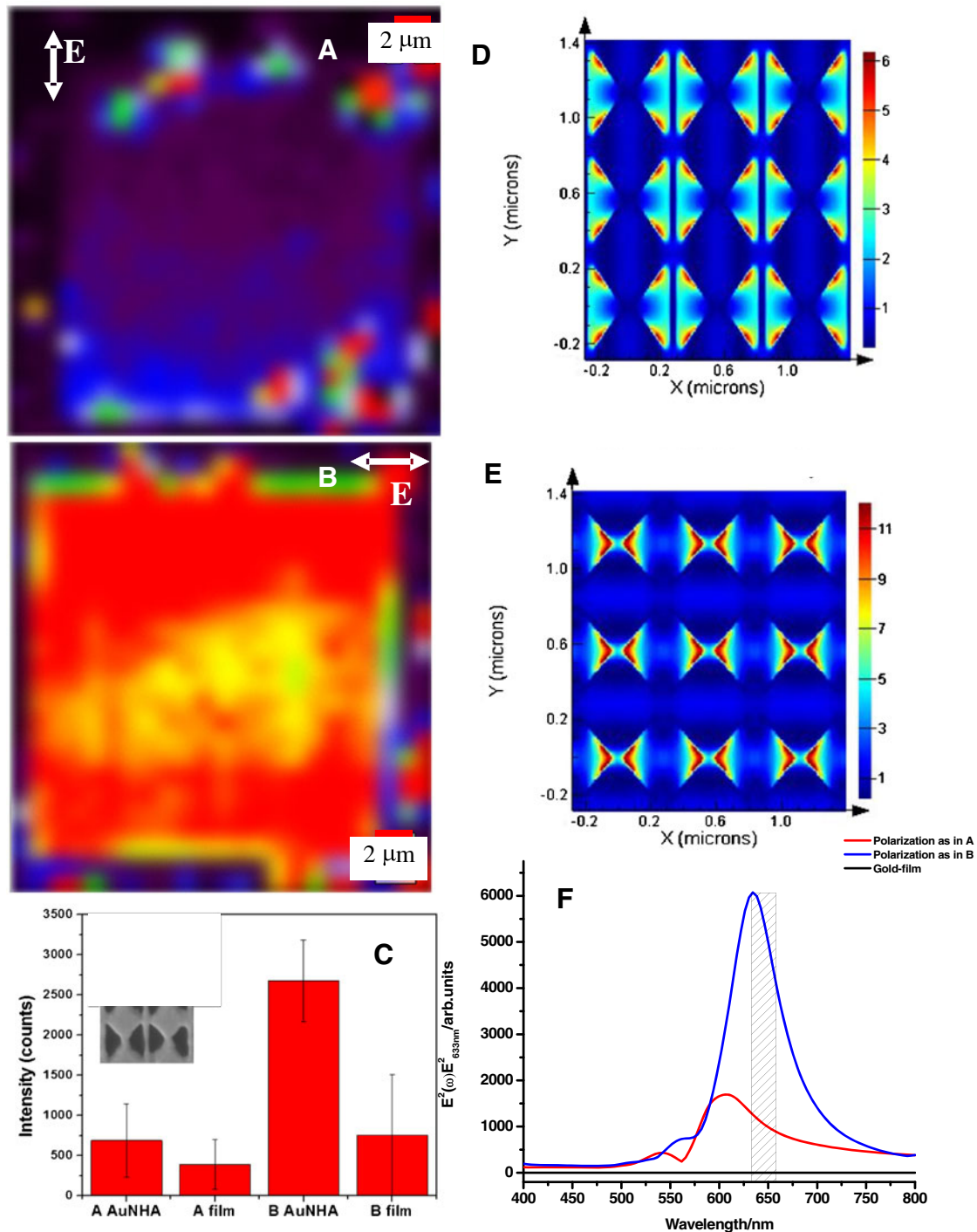
Fig. 4 **a** Mapping of the Oxa 594 cm^{-1} SERRS intensity on the bow tie AuNHA-OFT using the laser polarization indicated; **b** SERRS mapping for the polarization perpendicular to the first one, as indicated; **c** histograms with average SERRS intensity on the bow tie AuNHA and on the surrounding gold film for the polarizations in the items **a** and **b**. The *error bars* correspond to the standard deviation in the average intensity. The *insert* shows the orientation of the bow tie structures in these experiments; **d**, **e** near-field strength distribution obtained by FDTD for arrays of bow tie-shaped holes excited at 633 nm with polarizations parallel and perpendicular to the bow tie basis, respectively; **f** SERS enhancement factor, calculated as $(E(\omega)^2 E(633 \text{ nm})^2)$, plotted against the wavelength

The dependence of the SERRS intensity on the laser polarization occurs because the bow tie nanostructures are anisotropic. For anisotropic nanostructures, the local field localization will depend on the polarization of the light

relative to the regions with sharp regions [37, 38]. For the bow tie structures, the sharp apex of the triangles are separated by 95 nm, and the electric field will be strongly enhanced in this region for the polarization parallel to the inter-triangles axis, but the enhancement will be much lower for the perpendicular polarization. FDTD simulations were carried out to confirm both the polarization dependence and the central role of localized surface plasmon resonances on the SERRS results. Figure 4d, e shows the distribution of the electric near-field strength for the bow tie structures from both polarizations. The field localized at the tips of the structures excited with laser light polarized perpendicular to the bow tie basis is clearly stronger, leading to more efficient SERRS. SERS enhancement factors, evaluated as the product of the field intensity at the laser (633 nm) and at arbitrary Raman scattering frequencies (ω) ($E(\omega)^2 E(633 \text{ nm})^2$), obtained for both polarization by FDTD, are plotted against the wavelength in Fig. 4f (the shadowed area highlighted the range of wavelengths that encompass the Stokes scattering bands of the molecular probe Oxa). The calculations predict a fourfold more efficient scattering for the polarization perpendicular to the basis of the bow tie. The results from Fig. 4d–f match well with the experimental findings (Fig. 4c) that shows a 3.6 polarization ratio for Oxa adsorbed on the bow tie structures.

Reilly et al. showed that the SERS enhancement by the NHA on Ag is about 2 orders of magnitude higher than the enhancement observed from the thermally deposited metal film for the forward-scattering geometry (using a planar Ag substrate rather than optical fibers) [41]. The smaller enhancement of the nanostructure relative to the rough gold film observed here might be related to the additional resonance Raman contribution expected from our molecular probe (Oxa). The SERRS enhancement factor calculated relative to the resonance Raman effect is generally lower than the SERS enhancement factor calculated relative a species without the resonance effect [42]. The underestimated SERRS enhancement factor compared to the non-resonant situation has been attributed to the intrinsically large Raman cross section under resonance Raman conditions and to contributions due to the light absorption since the excitation energy is close to an intrinsic electronic transition in this case.

An additional contribution to the smaller difference between the patterned and unpatterned film than observed before in the literature might come from the relatively high roughness of the thermally deposited film on the optical fiber tip. An introduction of an annealing step to smooth the film before the fabrication of the arrays could minimize this contribution. This is certainly a parameter that needs to be optimized in future experiments.

The second measurement geometry for the SERRS experiments using optical fibers was the forward-scattering

(Fig. 2). Figure 5a presents SERRS spectra from an AuNHA-OFT in forward-scattering geometry with and without modification with Oxa. A broad feature centered around 460 cm^{-1} is present in both spectra, and it can be assigned to the normal Raman scattering from the glass material of the optical fiber [43]. The spectrum of the AuNHA-OFT modified with Oxa, presented in Fig. 5a,
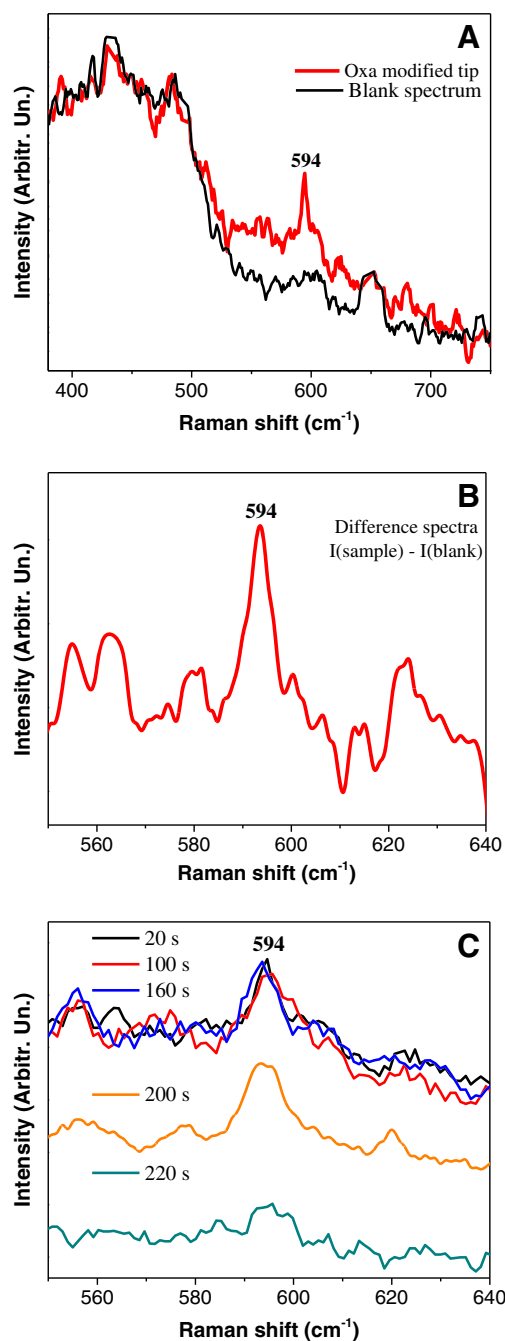

Fig. 5 **a** Spectra from the unmodified and Oxa-modified AuNHA-OFT, as indicated; **b** difference spectrum between an AuNHA-OFT before and after modification with Oxa; **c** time-dependent photodecompostion of an Oxa-modified AuNHA-OFT

shows the broad features from the glass and an additional band at 594 cm^{-1}, which is the most intense SERRS band of the phenoxazine ring of the dye [21]. In order to eliminate the glass background, the difference between the spectra from Fig. 5a was computed and is presented in Fig. 5b. In order to further demonstrate that the feature in Fig. 5b is due to Oxa, the laser power was increased to 4 mW and the dependence of the SERRS spectra with time was recorded. In these conditions, the SERRS intensity of the band at 594 cm^{-1} decreased with time, as shown in Fig. 5c. It can be noticed that the band at 594 cm^{-1} is virtually unchanged for the spectra between 20 and 160 s, but for the spectra at 200 s, the intensity of the band decreases, and for 240 s the band at 594 cm^{-1} cannot be observed anymore. Oxa absorbs in the region of the laser excitation and the decrease in the SERRS intensity is attributed to the photodegradation of the dye. The local photodegradation (only at the tip of the fiber) was further confirmed by Raman mapping in back-scattering mode, which showed that the SERRS signal of the Oxa disappeared at the fiber core region after this treatment (not shown). Similar results were obtained for the bow tie-shaped nanoapertures.

The observation of SERS spectra in the forward experiment for the AuNHA-OFT device is an interesting result because just the light that actually goes through the AuNHA due to extraordinary optical transmission excites the adsorbed molecules [36]. The SERRS data presented in Fig. 5 are encouraging, but the quality of the SERS signal reflected through the fiber was not very high and presented a low S/N ratio. SERRS experiments in optrode mode, where both the excitation and the scattering are measured at the distal (unmodified) fiber tip, were also attempted, but the quality was too low, due to the strong normal Raman from the glass that overwhelmed the SERRS signal from the probe molecule. The optrode configuration is the ultimate goal for applications of this type of fibers as remote SERS sensors in analytical chemistry. Although this configuration has been achieved for SERS in optical fibers modified with random nanostructures [30], further work in the direction of optimizing geometric parameters [35, 37, 38], such as tip-to-tip separation and structure dimensions, are required to obtain a similar level of enhancement from organized nanofabricated structures. In addition, further optimization of the thickness and smoothness of the Au layer might be required to improve both the coupling of the excitation with the adsorbed molecules at the tip of the fiber and the back-coupling of the scattered light into the fiber for detection.

Conclusions

Au nanoholes arrays were milled on gold films deposited on the tip of single-mode optical fibers. The device have been used as a SERRS substrate in both back- and forward-scattering, showing promising performance for both detection geometries. The effect of the nanoapertures shape was explored by using arrays of bow tie-shaped holes. This anisotropic structure allows the polarization dependence of the enhancement to be demonstrated both experimentally and numerically. The enhancement factors relative to the probe molecule adsorbed on the unpatterned region of the fiber tip was not very high. However, it is important to point out that the Raman signal from the unpatterned film was already orders of magnitude larger than expected from normal Raman, due to the roughness of the gold film and the resonance Raman effect.

Future work on this class of substrates will include the optimization of the nanostructures shape, size, tip-to-tip separation, and film thickness. The work on this direction would require a systematic optimization of fabrication conditions, which may take the substrate reported in this proof-of-concept manuscript to a new level of SERS/SERRS performance. The main goal is to produce a device that will provide enough enhancement from the adsorbed species that will allow optrode SERS measurements.

References

1. Wolfbeis OS (2006) Anal Chem 78:3859
2. Bello JM, Narayanan VA, Stokes DL, Vodinh T (1990) Anal Chem 62:2437
3. Mullen KI, Carron KT (1991) Anal Chem 63:2196
4. Fleischmann M, Hendra PJ, McQuillan AJ (1974) Chem Phys Lett 26:163
5. Jeanmaire DL, Vanduyne RP (1977) J Electroanal Chem 84:1
6. Albrecht MG, Creighton JA (1977) J Am Chem Soc 99:5215
7. Brolo AG, Irish DE, Smith BD (1997) J Mol Struct 405:29
8. Wu DY, Li JF, Ren B, Tian ZQ (2008) Chem Soc Rev 37:1025
9. Kneipp J, Kneipp H, Kneipp K (2008) Chem Soc Rev 37:1052
10. Leger C, Bertrand P (2008) Chem Rev 108:2379
11. Han XX, Chen L, Ji W, Xie Y, Zhao B, Ozaki Y (2011) Small 7:316
12. Pallaoro A, Braun GB, Reich NO, Moskovits M (2010) Small 6:618

13. Kneipp K, Wang Y, Kneipp H, Perelman LT, Itzkan I, Dasari R, Feld MS (1997) Phys Rev Lett 78:1667
14. Nie SM, Emery SR (1997) Science 275:1102
15. Hudson SD, Chumanov G (2009) Anal Bioanal Chem 394:679
16. Bell SEJ, Sirimuthu NMS (2008) Chem Soc Rev 37:1012
17. Fan M, Andrade GFS, Brolo AG (2011) Anal Chim Acta 693:7
18. Aroca R (2006) Surface-enhanced vibrational spectroscopy. Wiley, New York
19. Le Ru EC, Etchegoin PG (2009) Principles of surface-enhanced Raman spectroscopy: and related plasmonic effects. Elsevier, Amsterdam
20. Kelly KL, Coronado E, Zhao LL, Schatz GC (2003) J Phys Chem B 107:668
21. Brolo AG, Sanderson AC (2004) Can J Chem-Revue Canadienne De Chimie 82:1474
22. Brolo AG, Addison CJ (2005) J Raman Spectrosc 36:629
23. Vo-Dinh T, Stokes DL (2002) In: Chalmers JM, Griffiths PR (eds) Handbook of vibrational spectroscopy. Wiley, Chichester, p 1302
24. Stoddart PR, White DJ (2009) Anal Bioanal Chem 394:1761
25. Homola J, Yee SS, Gauglitz G (1999) Sensors Actuators B-Chem 54:3
26. Sharma AK, Jha R, Gupta BD (2007) IEEE Sensors J 7:1118
27. Guieu V, Lagugne-Labarthet F, Servant L, Talaga D, Sojic N (2008) Small 4:96
28. Andrade GFS, Brolo AG (2012) In: Dmitriev A (ed) Nanoplasmonic sensors. Springer, New York, p 289
29. Stokes DL, Vo-Dinh T (2000) Sensors Actuators B-Chem 69:28
30. Andrade GFS, Fan M, Brolo AG (2010) Biosens Bioelectron 25:2270
31. Zheng XL, Guo DW, Shao YL, Jia SJ, Xu SP, Zhao B, Xu WQ, Corredor C, Lombardi JR (2008) Langmuir 24:4394
32. Kostovski G, White DJ, Mitchell A, Austin MW, Stoddart PR (2009) Biosens Bioelectron 24:1531
33. Smythe EJ, Dickey MD, Bao J, Whitesides GM, Capasso F (2009) Nano Lett 9:1132
34. Brolo AG, Gordon R, Leathem B, Kavanagh KL (2004) Langmuir 20:4813
35. Brolo AG, Arctander E, Gordon R, Leathem B, Kavanagh KL (2004) Nano Lett 4:2015
36. Gordon R, Sinton D, Kavanagh KL, Brolo AG (2008) Acc Chem Res 41:1049
37. Lesuffleur A, Kumar LKS, Brolo AG, Kavanagh KL, Gordon R (2007) J Phys Chem C 111:2347
38. Min Q, Santos MJL, Girotto EM, Brolo AG, Gordon R (2008) J Phys Chem C 112:15098
39. Dhawan A, Muth JF, Leonard DN, Gerhold MD, Gleeson J, Vo-Dinh T, Russell PE (2008) J Vac Sci Technol B 26:2168
40. Kovacs GJ, Loutfy RO, Vincett PS, Jennings C, Aroca R (1986) Langmuir 2:689
41. Reilly TH, Chang SH, Corbman JD, Schatz GC, Rowlen KL (2007) J Phys Chem C 111:1689
42. Tarcha PJ, DeSaja-Gonzalez J, Rodriguez-Llorente S, Aroca R (1999) Appl Spectrosc 53:43
43. Pristinski D, Du H (2006) Opt Lett 31:3246